JOURNAL OF THERMOPHYSICS AND HEAT TRANSFER
Vol. 7, No. 2, April–June 1993

Monte Carlo Simulation of Entry in the Martian Atmosphere

David B. Hash* and H. A. Hassan†
North Carolina State University, Raleigh, North Carolina 27695

The Direct Simulation Monte Carlo (DSMC) method of Bird is used to investigate the characteristics of low density hypersonic flowfields for typical aerobrakes during Martian atmospheric entry. The method allows for both thermal and chemical nonequilibrium. Results are presented for a 60-deg spherically blunt cone for various nose radii and altitudes.

Introduction

AEROBRAKING has been proposed as an efficient means of reducing the required takeoff weight of spacecraft such as those envisioned for use in a Mars mission scenario.[1] One of the main concerns for such a scenario is the heating rates that an aerobrake will experience in its pass through the atmosphere. The heating rates will depend on the geometry of the aerobrake. Since the exact geometry of a Mars aerobrake has yet to be determined, this investigation concentrates on a shape similar to that used by Candler,[2] a 60-deg blunt cone. Most of the research conducted until now has been for low altitudes. At such altitudes, solutions to the Navier-Stokes equations are appropriate since the flow can be considered a continuum. The purpose of this work is to supplement previous research with results for higher altitude conditions for which the assumptions necessary for the derivation of the Navier-Stokes equations do not hold. Instead, the Direct Simulation Monte Carlo (DSMC) method of Bird[3] is used.

Physical Models

Instead of analyzing a mathematical model of the flow, DSMC simulates the flow through the computational movement and collision of particles. In this simulation the collision processes must be modeled accurately. The following discusses the collision, chemical reaction, and energy exchange models necessary to accurately model the hypersonic shock layer on a craft entering the Martian atmosphere.

Collision Model

The movement and collision of particles are decoupled over a small time step, and the flowfield is partitioned into several thousand cells in which the collision process is executed. The particles are moved over the small time step according to the equation

$$\frac{\mathrm{d}x}{\mathrm{d}t} = v \tag{1}$$

After all particles are moved, the collision procedure is enacted in each computational cell. Choices for collision partners must be determined. Instead of checking every collision pair possible in each cell, collision pairs are chosen at random. The probability for a collision is derived as a function of the collision cross section and the relative velocity of the collision partners. Once the probability is calculated it is compared to a random number. The collision occurs if the probability is larger than the random number. This is the so-called acceptance-rejection method and is repeated until an apropriate number of collision pairs (specified by the collision frequency and the time step) is chosen.

Now that the collision procedure has been introduced, the steps involved in the replication of postcollision phenomena can be described. First, a determination is made as to whether a reaction has occurred through the use of an appropriate chemical reaction model. Secondly, the probability of energy partitioning between the collision partners is calculated through the use of an appropriate energy exchange model. Both these models and the refinements necessary for accurate simulation of the Martian atmosphere will now be discussed.

Chemical Reaction Model

After a collision has occurred, a determination as to whether a reaction takes place must be made. The probability for reaction is termed the "steric factor" and is derived to reproduce available reaction rate data. The reaction rate can be derived from kinetic theory as a function of the product of the collision frequency, the steric factor, and the fraction of collisions with energy along the line of centers greater than the activation energy. The steric factor is chosen so that at equilibrium it reproduces an Arrhenius form for the reaction rate coefficient. The resulting expression of the steric factor is a function of the relative energy of the collision partners. Assumptions must be made about the contribution of the internal degrees of freedom (DOF) of the collision partners to the energy necessary to initiate a reaction. For this study it is assumed that half of the rotational and vibrational energy contribute. It is known that part—but not all—of the internal energy modes contribute to the energy of the reaction. The choice of a half is just a compromise. If the energy available is greater than the activation energy, a steric factor is calculated. Once again, the acceptance-rejection method is employed whereby the steric factor is compared to a random number to determine if a reaction occurs.

Fifty-four different reactions are allowed for this simulation using the rate data of Evans, Schexnayder, and Grose,[4] and are given as follows:

$$\begin{gathered}
CO_2 + M \rightarrow CO + O + M \\
CO + M \rightarrow C + O + M \\
N_2 + M \rightarrow N + N + M \\
O_2 + M \rightarrow O + O + M \\
NO + M \rightarrow N + O + M \\
CO + N \rightleftarrows NO + C \\
CO + CO \rightleftarrows CO_2 + C \\
CO + O \rightleftarrows O_2 + C \\
N_2 + O \rightleftarrows NO + N \\
NO + CO \rightleftarrows CO_2 + N \\
NO + O \rightleftarrows O_2 + N \\
CO_2 + O \rightleftarrows O_2 + CO
\end{gathered} \tag{2}$$

where M is any of the other species present.

Received Nov. 4, 1991; presented as Paper 92-0494 at the AIAA 30th Aerospace Sciences Meeting, Reno, NV, Jan. 6–9, 1992; revision received Feb. 17, 1992; accepted for publication Feb. 20, 1992.

*Research Assistant, Mechanical and Aerospace Engineering. Student Member AIAA.

†Professor, Mechanical and Aerospace Engineering. Associate Fellow AIAA.

Internal Energy Exchange Model

For each simulated physical process discussed to this point, a probability of occurrence has been given. One last physical process remains to be discussed, that of the internal energy exchange between the collision partners. A finite time is required for any energy mode to relax or equilibrate. This relaxation time is a function of the local flow properties and can be related to the number of collisions it takes for a particular mode to relax. This number of collisions is termed the relaxation number for that mode. Once this number is determined, the probability of relaxation for each mode in a given collision can be computed. This probability is defined as

$$(1/Z) = (1/v\tau) \tag{3}$$

where Z is the relaxation number, v is the collision frequency, and τ is the relaxation time.

It is necessary to specify the relaxation numbers for the rotational and vibrational modes in order to compute the relaxation probabilities. The number of collisions that is needed for the rotational mode to relax is chosen to be five. Studies by Olynick[5] have been conducted where this number was allowed to be a function of temperature. Those results do not show significant change with this modification, so the present results are calculated with a constant rotational relaxation number. However, the vibrational relaxation number is computed as a function of the flow properties. The relaxation number can be easily determined if the collision frequency and the relaxation time are known. Thus, in this work the Millikan and White[6] expression is used to determine the vibrational relaxation time for any species and is given by

$$\tau = \tau_L + \tau_{cs} \tag{4}$$

where

$$\begin{aligned} \tau_L &= (1/p)\exp[A(T^{-1/3} - 0.015\mu^{1/4}) - 18.42] \\ A &= 1.16 \times 10^{-3}\mu^{1/2}\Theta_v^{4/3} \end{aligned} \tag{5}$$

$$\begin{aligned} \tau_{cs} &= (1/c_s\sigma_v n_s) \\ c_s &= \sqrt{(8kT/\pi m_s)}, \quad \sigma_v = 10^{-21}(50{,}000/T)^2, \text{ m}^2 \end{aligned} \tag{6}$$

In the above equation p and T are the pressure and temperature; μ is the reduced mass of the collision partners; k is the Boltzmann constant; c_s, m_s, and n_s are the average thermal velocity, mass, and number density of species s, respectively; and Θ_v is the characteristic temperature of the vibrational mode of the diatomic species. τ_{cs} is a correction factor suggested by Park[7] as a limit, since the Millikan and White formula gives unrealistically small relaxation times for high temperatures. In most cases, Park's correction is not needed, because the vibrational relaxation number is not allowed to be less than the rotational relaxation number.

The Martian atmosphere is 95% carbon dioxide. CO_2 is a linear triatomic molecule with three vibrational modes: 1) a degenerate bending mode (θ_v = 945 K); 2) a symmetric stretching mode (θ_v = 1903 K); and 3) an asymmetric stretching mode (θ_v = 3329 K). Because θ_v for the bending mode is the smallest, most of the vibrational energy of CO_2 at the lower temperatures is in this mode. Moreover, this mode is in resonance with the stretching modes resulting in fast vibration-vibration energy exchange. As a result it was found that Eq. (5), with θ_v being the characteristic temperature of the bending mode, approximates well the measurements of Camac[8] and measurements compiled by Massey[9] (Fig. 1). As a result, the above-mentioned procedure is used to estimate the vibrational relaxation time of CO_2.

With the appropriate models, the collision rates, reaction rates, and relaxation rates can be accurately reproduced, and the microscopic properties of the flowfield can be determined. We, however, are interested in the macroscopic properties of density, temperature, heat transfer, etc. To acquire these characteristics of the flow, the microscopic properties are averaged over the particles in a given cell to give the macroscopic properties. Through this procedure, DSMC can be used to effectively simulate flowfields in the presence of thermal and chemical equilibrium or nonequilibrium.

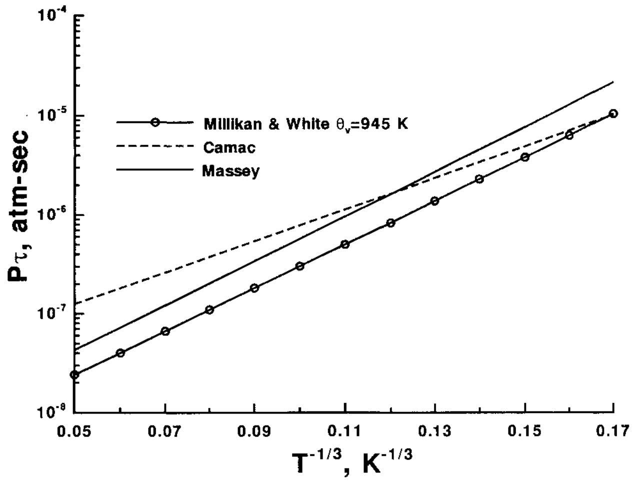

Fig. 1 Vibrational relaxation time for CO_2.

Results and Discussion

The main consideration when using DSMC is the amount of computational time required for a given set of freestream conditions. The computational time is directly related to the required number of computational cells. The dimension of each cell in the direction of high gradients must be less than a mean free path in order to accurately capture the gradients of the flow. Thus, DSMC is well-suited for flows in the transitional flow regime where the Knudsen number (the mean free path divided by a relevant scale length for the flow), is greater than 0.1 and the grid requirements are less stringent. At trajectory points for which the flow is a continuum, the mean free path is so small that the grid requirements result in large computational times. Therefore, a boundary between the continuum and transition regimes was employed to determine at what altitudes and entry velocities DSMC would be feasible. The boundary can be derived as a function of entry velocity and body dimension by the following relationship:

$$(u/L) = 1.435 \times 10^8 Kn^2 \rho \sqrt{T} \ \text{ s}^{-1} \tag{7}$$

where u is the entry velocity, L is the characteristic body dimension, Kn is the Knudsen number, T is the temperature, and ρ is the density at a given altitude. This equation is specific to the Martian atmosphere and is derived from the definition of the Knudsen number where

$$Kn = (\lambda/\delta) \tag{8}$$

In the above equation λ is the mean free path and δ is the boundary-layer thickness.

After plotting the function vs altitude (Fig. 2), altitudes were chosen so that the grid requirements are not excessive for DSMC. Three different altitudes were chosen; 60, 70, and 80 km in the Martian atmosphere as denoted in Fig. 2. The entry velocity is assumed constant and is 7.387 km/s for all cases in order to isolate the effects of altitude and body shape. Two nose radii are examined; 1.0 and 2.3 m for a 60-deg spherically blunt cone at 80 km. Calculations at 70 and 60 km are carried out on the 2.3-m case only. The wall temperature is fixed at 1000 K and the surface is partially catalytic. Recombination of oxygen and nitrogen atoms can occur at the surface, but no such mechanism is included for carbon monoxide. Given these conditions, the effects of body shape and altitude will now be discussed.

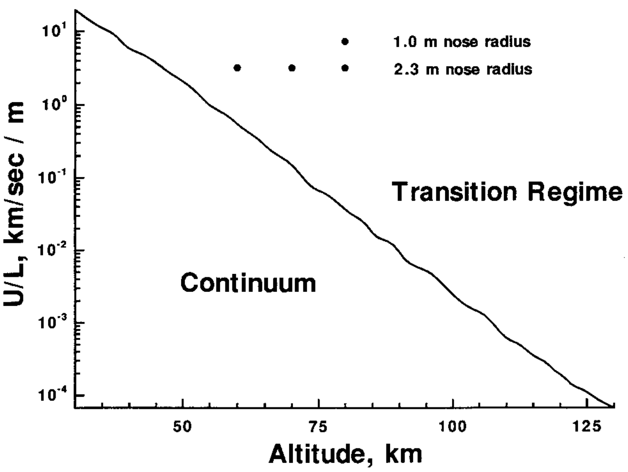

Fig. 2 Boundary between the continuum and transition regimes.

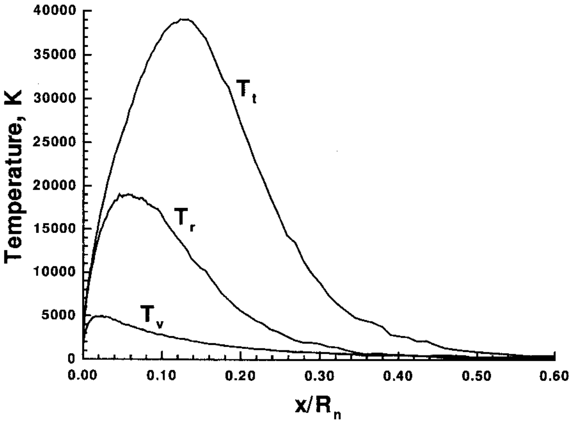

Fig. 3 Temperature profiles along stagnation streamline at 80 km for R_n = 1.0 m.

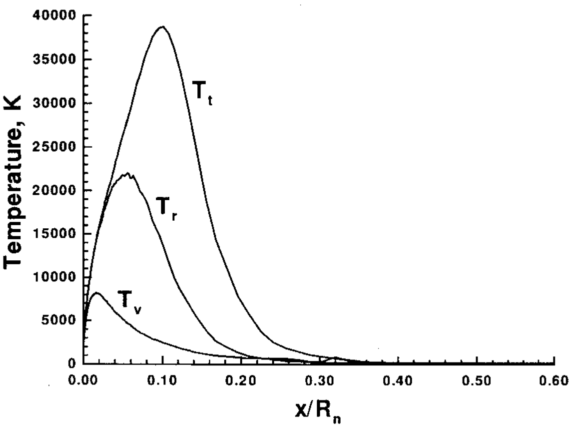

Fig. 4 Temperature profiles along stagnation streamline at 80 km for R_n = 2.3 m.

Figures 3 and 4 show the temperature profiles along the stagnation streamline at 80 km for the 1.0- and 2.3-m nose radius cases, respectively. For these cases, the Knudsen numbers are 1.08 and 0.713, respectively, the grid is 150 × 30, and 60,000 computational particles were employed. In the figure, x is the distance along the stagnation streamline and R_n is the nose radius. The temperature subscripts t, r, and v refer to the translational, rotational, and vibrational modes. At this altitude the shock is very diffuse. Because of the low density, the flow behind the shock never reaches thermodynamic equilibrium for the 80-km cases. The larger nose radius geometry has a larger shock detachment distance and thus a larger reaction zone. Also, the translational temperature peak is slightly lower for the 2.3-m nose radius body. Figures 5 and 6 show the temperature profiles at 70 and 60 km, respectively, for the 2.3-m nose radius body. For these cases, the Knudsen numbers, grid size, and computational particles are 0.355 and 0.188; 300 × 30, 400 × 30; and 135,000, 200,000, respectively. For both the 70- and 60-km altitudes, the flow reaches a quasithermodynamic equilibrium behind the shock characterized by a slight vibrational temperature overshoot. This overshoot is indicative of the source of the energy of reaction that results in dissociation. If more is contributed by translational and rotational energy, then the respective temperatures will be lower than the vibrational temperatures. The results suggest that a fraction of the vibrational energy larger than a half could have contributed to the energy of the reaction. With increasing density, the shock lies closer to the body, the thickness of the shock decreases, and the translational temperature peak continues to decay.

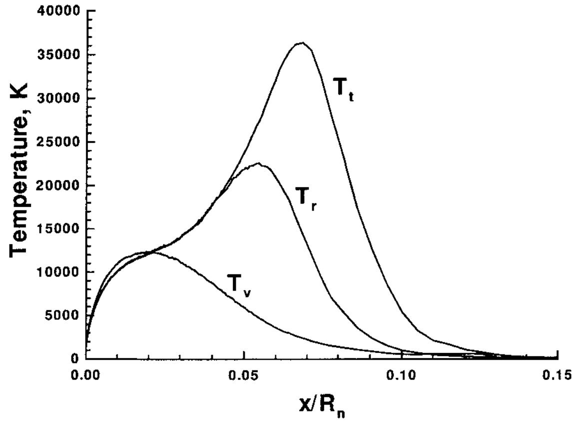

Fig. 5 Temperature profiles along stagnation streamline at 70 km for R_n = 2.3 m.

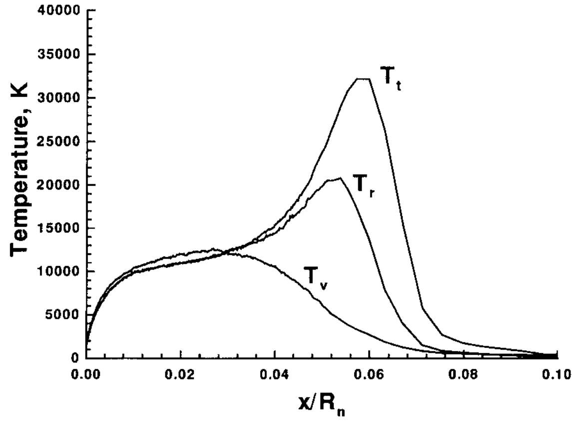

Fig. 6 Temperature profiles along stagnation streamline at 60 km for R_n = 2.3 m.

The temperature distributions in Fig. 6 are close to the expected results for a continuum solution where the mean free path is so small that the shock properties change almost discontinuously. Because the fraction of the shock detachment distance over which an appreciable difference between the rotational and translational temperature exists decrease with altitude, it appears that the assumption of rotational-translational equilibrium made by Candler for the continuum calculations is a good approximation.

Figures 7–10 show the mass fractions along the stagnation streamlines for the different cases. From Figs. 7 and 8 a significant increase in the amount of dissociation is seen for bodies with larger nose radius. This is a result of the larger detachment distance for the 2.3-m nose radius geometry. With the larger shock detachment distance, a larger reaction zone exists, and thus, dissociation reactions have more time to occur. The increase in dissociation is the reason for the trans-

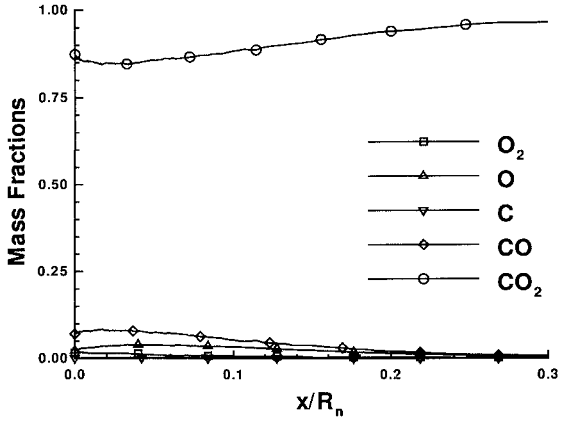

Fig. 7 Temperature profiles along stagnation streamline at 60 km for R_n = 2.3 m.

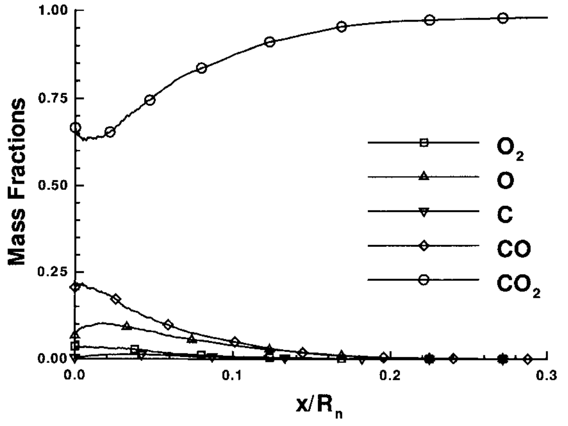

Fig. 8 Mass fractions along stagnation streamline at 80 km for R_n = 2.3 m.

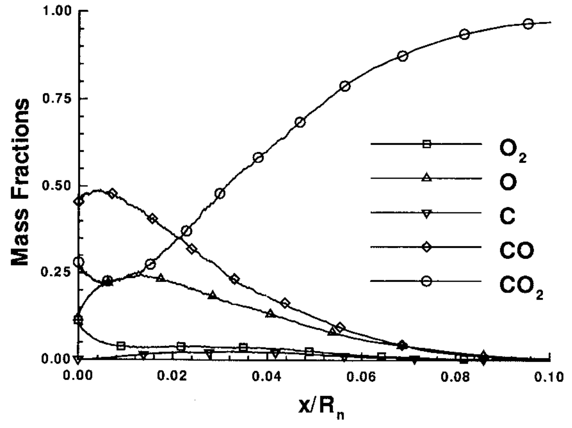

Fig. 9 Mass fractions along stagnation streamline at 70 km for R_n = 2.3 m.

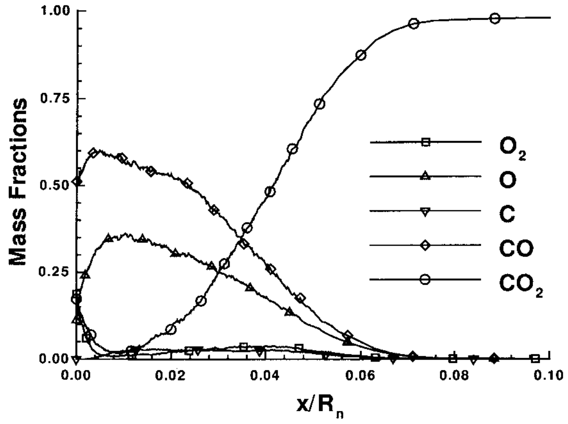

Fig. 10 Mass fractions along stagnation streamline at 60 km for R_n = 2.3 m.

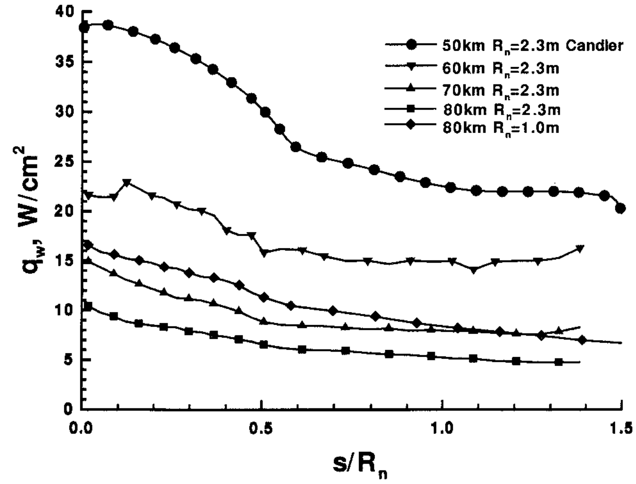

Fig. 11 Heat transfer rate along surface.

lational peak decay, because energy is being removed from the translational mode in the form of chemical energy. Figures 9 and 10 show an increased amount of dissociation with increased density. Because of the larger density, the collision frequency is higher which results in an increased amount of dissociation. Once again, the increase in dissociation is the reason for the translational temperature drop.

Figure 10 shows complete dissociation of CO_2 at 60 km for the 2.3-m nose radius geometry. Candler shows complete dissociation for a similar geometry at 50 km with the same entry velocity. Thus, these results are not unexpected.

For high Mach number boundary-layer flows,[10] the stagnation point heat transfer in air is inversely proportional to the square root of the nose radius. Thus, the convective heat transfer rate is reduced with a larger nose radius. Figure 11 shows the convective heat transfer rates for the various cases. In the figure, s represents the distance along the surface from the stagnation point. As expected, the heating for the 2.3-m nose radius geometry at 80 km is larger compared to the 1.0-m case. The figure also shows a larger heat transfer for lower altitudes or larger densities. Because of the larger number of particles impacting the surface and the larger collision frequency with the surface, more energy is imparted to the surface resulting in a larger heat transfer rate. The given results are for a partially catalytic wall for which nitrogen and oxygen atoms are allowed to recombine at the surface with a 2% probability. No allowance is made for the recombination of carbon monoxide at the surface. Thus, the results for the heating rates may underestimate the correct heating rates. Higher heating rates would be expected for a fully catalytic surface.

Included for comparison in Fig. 11 are Candler's results for a 60-deg ellipsoidally blunt cone at 50 km. Candler assumes a noncatalytic surface with the same fixed wall temperature as the above-described results. The same general trends can be seen.

Concluding Remarks

The amount of dissociation and the convective heat transfer rate will increase along the downward pass of the aerobrake because of the increased density. Although that part of the energy expended in dissociation increases with a decrease in altitude, the increase in heat transfer with a decrease in altitude is a result of increased particle flux to the surface.

Varying the geometry at 80 km shows significant effects on the amount of dissociation, thermal nonequilibrium, and heat transfer. Increasing the nose radius increases the shock detachment distance, and therefore, the reaction zone. As a result, dissociation reactions have more time to occur. The larger shock layer also yields a larger region of thermal nonequilibrium. And finally, as expected, the convective heat transfer rate decreases as the nose radius increases.

For altitudes and geometries considered here, a significant amount of thermal nonequilibrium between all energy modes is exhibited. Based on our results it appears that the assumption of translational-rotational equilibrium employed by Candler for continuum calculations is a good approximation.

Acknowledgments

This work is supported in part by a National Science Foundation Graduate Fellowship, NASA's Cooperative Agreement NCCI-112, the Hypersonic Aerodynamic Program Grant NAGW-1022 funded jointly by NASA, AFOSR, and ONR, and the Mars Mission Research Center funded by NASA Grant NAGW-1331. The authors acknowledge many helpful discussions with Graham V. Candler.

References

[1] Braun, R. D., "The Effect of Interplanetary Trajectory Options on a Manned Mars Aerobrake Configuration," M.S. Thesis, George Washington Univ., Washington, DC, Aug. 1989.

[2] Candler, G. V., "Computation of Thermo-Chemical Nonequilibrium Martian Atmospheric Entry Flows," AIAA Paper 90-1695, June 1990.

[3] Bird, G. A., *Molecular Gas Dynamics*, Clarendon Press, Oxford, England, UK, 1976.

[4] Evans, J. S., Schexnayder, C. J., and Grose, W. L., "Effects of Nonequilibrium Ablation Chemistry on Viking Radio Blackout," *Journal of Spacecraft and Rockets*, Vol. 11, No. 2, 1974, pp. 84–88.

[5] Olynick, D. P., Moss, J. N., and Hassan, H. A., "Monte Carlo Simulation of Nonequilibrium Shock Fronts," AIAA Paper 91-1341, June 1991.

[6] Millikan, R. C., and White, D. R., "Systematics of Vibrational Relaxation," *Journal of Chemical Physics*, Vol. 39, No. 12, 1963, pp. 3209–3213.

[7] Park, C., "Assessment of a Two-Temperature Kinetic Model for Dissociating and Weakly Ionizing Nitrogen," *Journal of Thermophysics and Heat Transfer*, Vol. 2, No. 1, 1988, pp. 8–16.

[8] Camac, M., "CO_2 Relaxation Processes in Shock Waves," *Fundamental Phenomena in Hypersonic Flow*, edited by J. G. Hall, Cornell Univ. Press, Ithaca, NY, 1966, pp. 195–215.

[9] Massey, H. S. W., *Slow Collisions of Heavy Particles. Electronic and Ionic Impact Phenomena*, Vol. 3, Clarendon Press, Oxford, England, UK, 1971, pp. 1523–1526.

[10] Anderson, J. D., Jr., *Hypersonic and High Temperature Gas Dynamics*. McGraw-Hill, New York, 1989, pp. 626–636.